Microscopic Investigation of the Excitons' Intermolecular Energy Migration in the Phase of Poly(9,9-dioctylfluorene) by Confocal Laser Spectroscopy

ARTICLE *in* THE JOURNAL OF PHYSICAL CHEMISTRY C · FEBRUARY 2008

Impact Factor: 4.77 · DOI: 10.1021/jp074804d

3 AUTHORS, INCLUDING:

Marco Anni
Università del Salento
105 PUBLICATIONS **1,929** CITATIONS
SEE PROFILE

Sandro Lattante
Università del Salento
31 PUBLICATIONS **215** CITATIONS
SEE PROFILE

Microscopic Investigation of the Excitons' Intermolecular Energy Migration in the β Phase of Poly(9,9-dioctylfluorene) by Confocal Laser Spectroscopy

M. Anni,* M. E. Caruso, and S. Lattante

Dipartimento di Ingegneria dell'Innovazione, Università del Salento, Via per Arnesano 73100 Lecce, Italy

Received: June 20, 2007; In Final Form: December 13, 2007

We investigated, by confocal laser spectroscopy, the role of the microscopic morphology on the fluorescence spectra of poly(9,9-dioctylfluorene) (PF8) thin films self-doped by the PF8 β phase. We demonstrate the existence, on the micron scale, of different regions in the films, characterized by locally different fluorescence spectra. We show that the microscopic morphology irregularities lead to locally nonuniform β-phase density resulting in the switching on or off of the intermolecular energy migration within the β-phase excited-state distribution. This effect causes considerable local variation of the fluorescence spectra consisting of a progressive red shift (up to 26 meV) and a line width narrowing from about 70 (similar to the absorption one) down to 52 meV.

I. Introduction

In the past decade, a large research effort has been focused on the study of light-emitting organic conjugated polymers. This interest is strongly related to the possibility to use conjugated polymers in a wide family of photonic, optoelectronic, and electronic devices, like lasers,[1] light-emitting diodes (LEDs),[2] field effect transistors (FETs),[3] solar cells,[4] and light-emitting transistors (LETs).[5]

In order to fully exploit the qualities of conjugated polymers in device applications, a deep understanding of their photophysics and of the processes affecting it is fundamental.

An important peculiarity of organic polymers with respect to inorganic active materials is the positional and energetic disorder due to structural defects and to the entanglement of the polymer chains. Such disorder results in inhomogeneously broadened emission and absorption spectra and, more importantly, in the presence of local minima in the energy landscape. When a polymer is excited in states that are in the high-energy tail of the density of states, energy migration toward lower energy sites takes place (downhill migration[6,7]). This process leads the excitation toward lower energy until no sites at even lower energy are available in the close proximity, thus leading to excitation localization. At room temperature, uphill migration can also take place due to the possible thermal excitation toward higher-energy sites.[8]

A detailed investigation of the energy migration process is extremely important to understand, and optimize, the properties of polymers to be used in devices. For example, it has been shown that in some host−guest systems, usually employed in low-threshold lasers[9] and high-luminance LEDs,[10] energy migration in the host takes place between the host photoexcitation and the Förster Transfer to the guest, allowing a more efficient energy transfer toward low-energy-emitting guests.[11,12] In a similar way, in polymeric systems for solar cells application, the energy migration is a fundamental step between the photoexcitation and the charge separation.[13] On the other side, energy migration can have detrimental effects on the light emission efficiency, assisting energy transfer toward quenching centers,[14] chemical defects,[15] and low-efficiency emitters, like excimers, and on the solar cell efficiency due to energy migration toward charge traps.[16,17]

Moreover, in the past few years, several experiments investigating spatially resolved photoluminescence demonstrated that the emission properties of organic thin films can be strongly nonuniform across the film surface. In particular, near-field scanning optical microscopy (NSOM) experiments have been performed in order to study, with a resolution on the order of 100 nm, organic blends showing phase separation,[18−21] as well as the aggregation[22,23] and the photo-oxidation[24] in polyfluorene thin films. In a similar way, confocal laser spectroscopy, with a sub-micrometric lateral resolution, was recently employed to investigate the supramolecular organization of sexithiophene thin films[25] and to correlate the emission spectra of polyfluorene films to their microscopic morphology.[26]

Among the several existing families of conjugated polymers, polyfluorene-based compounds recently demonstrated extremely interesting properties already exploited in high-luminance LEDs,[27,28] solar cells,[29] transistors,[30] lasers,[31−33] and LETs.[34] Moreover, polyfluorenes are excellent systems for basic photophysics studies due to their mesomorphism[35] and to the strong morphology dependence of their emission properties.[26,36] In particular, two different phases, known as the glassy phase and the β phase, are usually present in thin films deposited from solution,[37] with a relative concentration that can be modified by acting on the deposition process,[38] or by postdeposition processes like thermal cycling[35,39] or exposure to solvent vapors.[40]

The presence of these distinct phases, attributed to different chain geometries,[41] makes polyfluorene a very interesting system to investigate the molecular structure dependence of several basic physics processes, like the triplet exciton formation,[42] the charge separation,[43] and the optical gain.[44] Finally, the polyfluorene β phase is a good system to investigate the environment dependence of the emission spectra due to an emission spectrum with unusually narrow features and an extremely well-resolved vibronic structure, in particular at low temperature.[35]

* To whom correspondence should be addressed. E-mail: marco.anni@unile.it.

10.1021/jp074804d CCC: $40.75
Published on Web 02/05/2008

Despite the several interesting properties of polyfluorenes, the known dependence of their emission properties on the film morphology, and the general importance of a deep understanding of the energy migration effects on the fluorescence spectra in organic films, no space-resolved investigations of these effects have been reported to date.

In this paper, we investigated by confocal laser spectroscopy the effects of microscopic morphology irregularities on the emission spectra of poly(9,9-dioctylfluorene) (PF8) thin films exposed to toluene vapors in order to induce the glassy $\rightarrow \beta$ phase transition, chosen as a prototypical host−guest system. We show that, on the few microns scale, different regions with individually different fluorescence spectra contribute to the sample emission. We conclude that the microscopic morphology irregularities lead to local variations of the β-phase molecule density, resulting in a locally nonuniform excitons' intermolecular migration within the β-phase excited-state distribution. This effect results in clear line shape differences between the fluorescence spectra collected from different sample regions, consisting of a progressive fluorescence red shift up to 26 meV, and in a line width narrowing from about 70 (similar to the absorption one) down to 52 meV.

II. Experimental Section

The PF8 was purchased from HW Sands and used as received. The glassy phase PF8 films have been prepared by spin coating from chloroform solution on glass. The samples have been then exposed to toluene vapors for 12 h in order to induce the glassy $\rightarrow \beta$ phase transition. The standard fluorescence measurements have been performed by exciting the samples with a continuous-wave He−Cd laser ($\lambda = 325$ nm, $E = 3.815$ eV). The fluorescence, collected by a telescopic lens system, has been dispersed by a TRIAX320 spectrometer and detected by a Jobin−Yvon silicon charge-coupled device (CCD). The fluorescence measurements with spatial resolution of about 1 μm were performed with an Olympus FV1000 confocal microscope by exciting the samples with a solid-state laser ($\lambda = 405$ nm). The fluorescence has been spectrally dispersed by a monochromator with 1 nm spectral resolution and detected by a photomultiplier. All the fluorescence measurements were performed with an excitation density of about 40 W cm^{-2} at room temperature in air. The absorption spectra were measured by a double beam spectrophotometer.

III. Results and Discussion

The fluorescence spectrum (excited at 3.815 eV) of the pristine sample (see Figure 1) shows the typical features of the PF8 glassy-phase emission with the 0−0 fluorescence resonance at about 2.930 eV and two low-energy shoulders, at about 2.797 and 2.601 eV, due to vibronic replicas.[40] After toluene vapor exposure, no signatures of glassy-phase emission are observed, and the fluorescence spectrum presents the typical features of β-phase fluorescence, with a 0−0 line at 2.807 eV, followed by vibronic replicas at about 2.665 and about 2.483 eV. The line width (LW) of the 0−0 β-phase line (defined as twice the standard deviation of the Gaussian best-fit curve) is 71.2 ± 0.7 meV. The absorption spectrum of the solvent-exposed samples shows two main resonances. The low-energy one, with a peak energy of 2.849 eV and a line width of 72.2 ± 1.6 meV, is attributed to the $S_0 \rightarrow S_1$ β-phase absorption line, while the broader band peaked at about 3.25 eV is due to the $S_0 \rightarrow S_1$ β transition of the glassy phase.[40] A total content of β phase of about 5.8% has been estimated from the absorption spectra.[40]

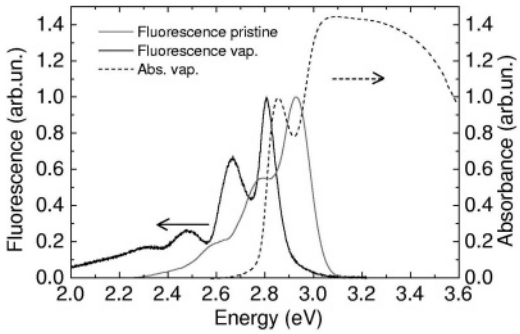

Figure 1. Standard fluorescence spectra of the PF8 film before (gray solid line) and after (black solid line) toluene vapor exposure. The fluorescence spectrum of the pristine film is typical of the PF8 glassy phase, while the one of the sample exposed to toluene vapors is typical of the PF8 β phase. The absorption spectrum (dark dashed line) shows the $S_0 \rightarrow S_1$ β-phase absorption peak at 2.849 eV and the glassy phase one at about 3.25 eV.

The fluorescence intensity map of samples exposed to toluene vapors usually shows a uniform intensity and line shape due to uniform morphology and uniform β-phase distribution in the film.[26] Nevertheless, in some sample regions of the typical size of some tens of microns, covering about 10% of the sample surface, clearly distinct domains can be observed (see Figure 2). In region 1 of Figure 2, the fluorescence map at 2.780 eV shows two distinct uniform zones with different fluorescence intensities, labeled C and D. In a similar way, in region 2 at 2.780 eV, four uniform zones with different fluorescence intensities can be distinguished (labeled B′, C′, D′, and D″). In order to investigate the origin of the local differences of the fluorescence intensity, we also measured the fluorescence maps at 2.844 eV, thus in the high-energy tail of the fluorescence spectrum.

Very interestingly, the variation of the detection energy allows us to observe locally different intensity variations. In particular, the fluorescence map at 2.844 eV of region 1 still shows a uniform signal in zone D and in part of zone C but also the presence of a dark region at the borderline between zones C and D (labeled zone B) and a second dark zone with irregular geometry within region C (labeled region A). Strong local differences of the fluorescence intensity dependence on the detection energy are also observed in region 2, showing that zone B′, the brightest at 2.780 eV, is almost dark at 2.844 eV, while a narrow bright zone (E′) can be observed between zones B′ and D′. The various different zones visible in the fluorescence map at 2.780 and 2.844 eV can also be distinguished in the excitation laser-scattered light maps (see Figure 2), showing microscopic morphology irregularities.

In order to have a deeper insight into the local differences in the fluorescence intensity dependence on the collection energy, we measured the fluorescence maps with collection energies between 2.572 and 2.995 eV, and we analyzed the fluorescence spectrum in 200 different regions of interest (ROI) with a circular shape and about 1 μm radius (see Figure 2). In Figure 3, we show five representative fluorescence spectra collected in the various ROI shown in Figure 2. Clear differences in the peak energy of the 0−0 line and in its line width can be observed. The fluorescence spectrum collected in the ROI D1 shows a 0−0 line peak energy (obtained from a Gaussian best-fit) of 2.8269 ± 0.0005 eV and a line width of 70 ± 1 meV. The fluorescence spectra collected in the other ROI show a red shift and a clear 0−0 line narrowing with respect to the ROI D1 one. In particular, the fluorescence spectrum of ROI B′1 shows a peak energy of 2.8013 ± 0.0004 eV, with a line width

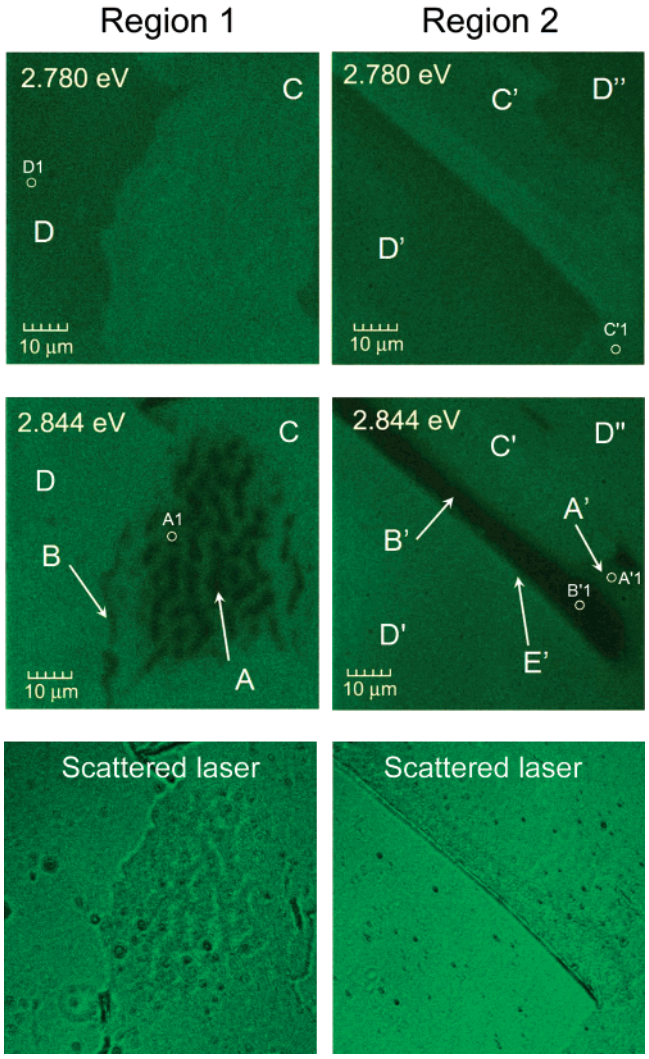

Figure 2. Top: A 69 × 69 μm^2 fluorescence intensity map at 2.780 eV in two different sample regions (left and right). Middle: A 69 × 69 μm^2 fluorescence intensity map in the same two regions on the top but at 2.844 eV. The locally different intensity variations between the two detection energies reflect local variations of the fluorescence spectra. Bottom: Scattered laser light map in the same two regions, evidencing the local microscopic morphology irregularities.

reduced to 53.2 ± 0.8 meV. It is important to observe that the 0−1 vibronic replica around 2.66 eV shows a shift similar to the 0−0 line one (see Figure 3), thus allowing us to rule out that the observed local variations of the fluorescence spectra are simply due to different self-absorption.

The investigation of the line shape dependence on the 0−0 peak energy (see Figure 3b) in all of the 200 ROI allows us to observe the following features: (1) The fluorescence line width LW linearly increase from about 52 to about 70 meV as the peak energy increases from about 2.801 to about 2.819 eV, while for higher-emission energies (up to 2.827 eV), the line width is almost constant with a value of about 70 meV, which is very close to the line width of the 0−0 peak of the β-phase absorption peak (about 72 meV). (2) The data relative to the same zone, identified from the fluorescence map of Figure 2, are not scattered across the line width−peak energy plot, but on the contrary, they are clearly grouped within a few meV. This indicates that within the same zone, the fluorescence spectra are very similar and suggests that the observed differences from zone to zone are likely related to the microscopic morphology irregularities of the sample. (3) The ensemble fluorescence

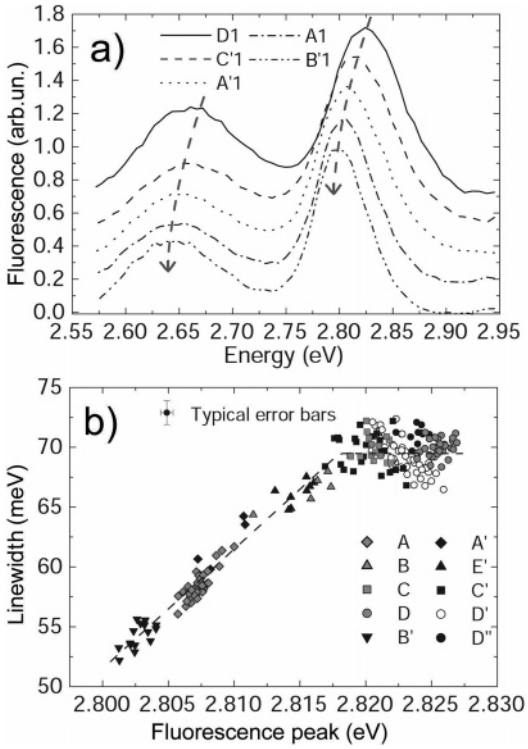

Figure 3. (a) Fluorescence spectra in five characteristic regions of the sample. It is evident that, from top to bottom, both the 0−0 line and the 0−1 line red shift by about 25 meV. A clear narrowing of the 0−0 line (from top to bottom) is also visible. The dark-gray arrow on the right is a guide for the eyes highlighting the 0−0 line red shift, while the arrow on the left is simply translated in order to show that the 0−1 line shift is comparable to the 0−0 one. (b) Fluorescence line width as a function of the fluorescence peak energy (dot). The line is the best fit curve with the fitting function described in the text.

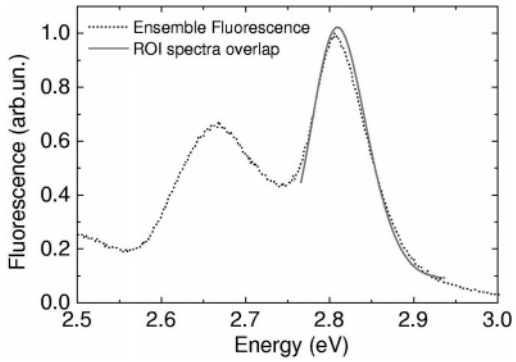

Figure 4. Comparison between the ensemble fluorescence spectrum (dark dotted line) and a linear combination of the spectra of ROIs A1 (30%), D1 (25%), A′1 (15%), B′1 (15%), and C′1 (15%), with relative weights in parentheses.

spectrum can be reproduced by a linear combination of the microscopic spectra (see Figure 4).

In order to quantify the line width dependence on the emission peak energy (E_P), we adapted, in the minimum χ^2 sense, the data to the following fitting function

$$\mathrm{LW} = \mathrm{LW}_{\max} + \frac{m}{2}(E_P - E_{P_0})\left(1 - \frac{|E_P - E_{P_0}|}{E_P - E_{P_0}}\right) \quad (1)$$

which is linear with slope m if $E_P < E_{P_0}$, while it is constant with a value of $\mathrm{LW}_{\max}$ if $E_P > E_{P_0}$. The best-fit curve (see Figure 3) is obtained for $m = 0.94 \pm 0.02$, $E_{P_0} = 2.8187 \pm 0.0006$ eV, and $\mathrm{LW}_{\max} = 69.7 \pm 0.3$ meV.

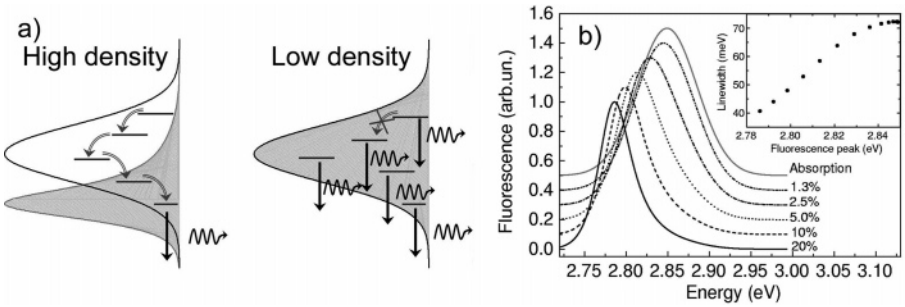

Figure 5. (a) Pictorial view of the β-phase density effects on the fluorescence spectrum. The black line represents the absorption spectrum, the gray arrows indicate the intermolecular energy migration, the black arrows represent the radiative relaxation, while the gray area is the fluorescence spectrum calculated for a β-phase content of about 20 (left) and about 1.3% (right), respectively. It is evident that a low β-phase content prevents energy migration before emission, thus leading to a broad fluorescence spectrum with the same line width as that of the absorption one, while a high β-phase content leads to a fluorescence red-shifted and narrowed with respect to the absorption. (b) Simulated fluorescence spectra as a function of the β-phase content. Inset: Fluorescence line width as a function of the fluorescence peak energy.

In order to explain the observed local fluorescence variation, it is important to remember that, in our experiment, the pump laser ($h\nu = 3.06$ eV) mainly excites molecules of the PF8 glassy phase. Then, as it has been already demonstrated in PFO films prepared with the same procedure as that of our samples,[40] energy migration within the excited-state distribution of the glassy phase and Förster resonant energy transfer (FRET)[35,40] to the β-phase molecules takes place[40] in less than 5 ps even at 5 K. Finally, intermolecular energy migration within the β-phase excited-state distribution usually takes place[40] in a typical time of about 25 ps at 5 K and a time shorter than 5 ps at room temperature.[40] Obviously, in parallel to any of the described steps, recombination, radiative or nonradiative, takes place.

In order to attribute the observed local variation of the fluorescence spectra, we observe that the macroscopic time-resolved experiment performed in ref 40 on a PF8 film containing the glassy and β phase demonstrates that the energy migration within the glassy phase and the FRET to the β phase are much faster than the β-phase emission, even at low temperature. It seems then unlikely that local morphology irregularities can slow down these processes taking place within the glassy phase to make them as slow as the β-phase emission.

On the other side, we observe that a fluorescence red shift and narrowing, qualitatively similar to our results, has been observed by time-resolved fluorescence measurements[8,12] under site-selective excitation. These experiments demonstrated that the excitation high in the absorption band leads to a fluorescence red shift and narrowing as the time after the excitation increases due to intermolecular energy migration within the excited-state distribution. On the contrary, the excitation at low energy creates excitons only on long conjugated segments, which basically do not migrate within their lifetime, thus emitting with time-independent energy and line width.

Despite this important similarity between the effects of energy migration on the temporal evolution of the fluorescence spectra and our results, we would like to stress the differences between the two physical situations. In the experiments of refs 8 and 12, the fluorescence variations with time are observed when the pulsed excitation energy is changed, while in our experiment, the excitation is continuous-wave and at a fixed energy (in a condition in which energy migration would be observed in a typical polymeric film), and the fluorescence differences are observed by looking at the spectra from different sample regions. However, despite the discussed differences in the two physical conditions, it is reasonable to attribute the observed results to local inhomogeneities of the exciton energy migration within the β-phase inhomogeneously broadened excited-state distribution. We observe that local variations of the β-phase molecule density lead to fluorescence spectra variations consistent with the experiment. Actually, if the density of β-phase molecules is too small to allow intermolecular energy migration within the β-phase density of states, the excitons, once transferred by FRET from the glassy to the β phase, cannot further migrate, as they are localized and thus recombine from the site initially excited by FRET (see Figure 5). The resulting fluorescence spectrum has then a line shape reflecting the inhomogeneously broadened energy distribution of the β phase, thus with the same line width of the absorption spectrum, and red-shifted with respect to the absorption due to a Stokes shift. On the contrary, a high density of β-phase molecules decreases the average β-phase distances at values allowing intermolecular energy migration within the β-phase molecules, thus causing a fluorescence red shift and narrowing (see Figure 5).

Concerning the formation process of the β-phase density irregularities, we observe that the fluorescence narrowing and red shift is observed in zones with a different morphology with respect to the surrounding regions, at the borderline between larger uniform regions (like region B and E′) or limited in lateral extension, in at least one dimension, to a few microns (like zone A and B′). It is known that microscopic morphology irregularities are characterized by a locally different, usually higher, surface energy, which results in a significant increase of nucleation processes[45−47] that are similar to the β-phase formation processes.[35,48] It is then likely that, in these regions, a stronger PF8 toluene vapor interaction leads to the formation of a higher number of molecules with the β-phase chain conformation, with respect to the surrounding uniform regions, thus explaining the observed local variations of the PL spectra. The proposed formation process of the β-phase density inhomogeneities, assisted by nonuniform solvent vapor pressure during the β-phase formation, is similar to the one recently exploited for nanopatterning of organic films and should be then controllable by artificially engineering the toluene vapor pressure over the film surface during the β-phase formation.[49] Moreover, we observe that this attribution is consistent with the close similarity of the PL spectra collected in different positions within zones with similar morphologies as the β-phase molecule density depends on the local morphology.

We finally observe that the maximum observed E_P variation, which we attribute to local variations of the intermolecular energy diffusion rate, is about 26 meV, which is in perfect agreement with the shift due to the β-phase intermolecular energy migration observed by time-resolved fluorescence in samples with a high β-phase total content (13%).[40] On the contrary, our results are not consistent with a local variation of the average β-phase conjugation length. In a simple particle in

a box picture, the emission energy is inversely proportional[50] to the conjugation length L; thus, the inhomogeneous LW for a fixed conjugation length distribution ΔL is LW $\propto |(dE)/(dL)| \Delta L \propto \Delta L/E^2$. An eventual decreased planarity of the β-phase molecules in the high-energy-emitting regions would then lead to an increase of LW quadratic, and not linear, and would not explain the LW plateau at energies higher than 2.82 eV.

In order to confirm our attribution, we used a simple, qualitative, model to investigate the intermolecular diffusion rate dependence of the fluorescence spectra of an inhomogeneously broadened system of randomly positioned molecules.

First of all, assuming a constant oscillator strength for all of the β-phase molecules, the energy distribution of the molecules is directly proportional to the 0−0 line of the absorption spectrum. Thus, the number of molecules with energy between E_i and $E_i + \Delta E$ is given by

$$g(E_i)\Delta E = \frac{n_0}{\sqrt{2\pi}\sigma} \exp\left(-\frac{(E_a - E_i)^2}{2\sigma^2}\right)\Delta E \qquad (2)$$

where n_0 is the total number of molecules, σ is the absorption standard deviation, and E_a is the absorption peak energy.

Moreover, as the excitation laser at $E_p = 3.06$ eV mainly excites the glassy-phase PF8 molecules, the β-phase molecules are not directly excited by the laser but are mainly indirectly excited by Förster resonant energy transfer (FRET) from the glassy phase.[40] As at room temperature the glassy $\rightarrow \beta$ phase transfer is very fast,[40] we assume that all of the β-phase molecules have the same probability of being excited. Thus, the number of excited molecules at any energy is directly proportional to the molecule number at that energy.

The excitation of the molecules is then followed by incoherent intermolecular energy migration and by relaxation. The rate equation of the population at energies between E_i and $E_i + \Delta E$ is given by

$$\frac{dn_i}{dt} = g(E_i)\Delta E + \sum_{j=1}^{i-1} R_{j,i} n_j - \sum_{j=i+1}^{N} R_{i,j} n_i - \frac{n_i}{\tau_{em}} \qquad (3)$$

where the first term describes the excitation from the glassy phase, the second describes the excitation from the β-phase molecules at higher energy, the third describes the de-excitation due to energy transfer to lower-energy β-phase molecules, while the last term describes monomolecular recombination.

Under steady-state conditions, the solution is given by

$$n_i = \frac{g(E_i)\Delta E + \sum_{j=1}^{i-1} R_{j,i} n_j}{\sum_{j=i+1}^{N} R_{i,j} + \frac{1}{\tau_{em}}} \qquad (4)$$

We considered, for simplicity, only downhill migration (energy migration toward molecules with lower energy) due to Förster-type energy transfer via dipole−dipole coupling

$$R_{i,j} = k_0 \left(\frac{R_0}{d_{i,j}}\right)^6 \qquad (5)$$

where k_0 is a frequency term and $d_{i,j}$ is the average distance between a molecule at energy E_i and a molecule at energy E_j, with $E_i > E_j$. In the model, we fixed $E_a = 2.849$ eV, $\sigma = 36.1$ meV, $\tau_{em} = 400$,[40] and we assumed uniform spatial distribution of the molecules. The simulated fluorescence spectra are reported in Figure 5b as a function of the relative β-phase molecules in the film.[51] For a β-phase content smaller than 1×10^{18} cm^{-3} (corresponding to a relative content of about 1.3%), the fluorescence spectra almost coincide with the absorption one, as the average distance between different β-phase molecules is so large as to make downhill energy migration much slower than the radiative relaxation, thus leading to molecules emitting at the same energy at which they are excited. When the β-phase content increases, the energy migration becomes progressively faster, and a fluorescence red shift and narrowing becomes evident. Moreover, the fluorescence line width dependence on the peak energy (inset of Figure 5), obtained from a Gaussian best fit of the simulated fluorescence spectra, is very similar to the experimental one, with a linear LW increase up to $E_{PL} \approx 2.836$ eV followed by a saturation, with an almost constant LW value of about 72 meV for 2.836 eV $< E_{PL} <$ 2.845 eV.

Concerning the quantitative agreement between the simulations and the experimental spectra, two main differences have to be commented upon. First of all, the maximum fluorescence peak energy from the simulation is identical to E_a, while the experimental one is about 18 meV lower (2.827 eV; see Figure 3). This disagreement is anyway expected as no Stokes shift is included in the model. In particular, it is well-known that, even in single molecules, the fluorescence is red-shifted due to structural relaxation between excitation and emission on the scale of tens of meV,[52,53] which is consistent with the observed disagreement between experiment and simulations.

Concerning the slope of the linear region of the LW dependence on E_{PL}, the theoretical best-fit value is 0.66 ± 0.01, which is about 30% lower than the experimental value of 0.94 ± 0.02. This is likely due to the underestimation of the contribution to the fluorescence of the molecules in the low-energy tail of the density of states due to the neglect of uphill energy migration. Actually, in our model, once the excitation has reached one of the low-energy-emitting molecules, the energy migration stops as there are few molecules at even lower energy, which are, on average, rather far apart. In the real situation, the excitation can be thermally transferred back to high-energy molecules and then migrate toward lower-energy sites. This uphill migration then increases the fluorescence contribution of the low-energy molecules, thus giving rise to a further narrowing of the fluorescence spectrum and to a higher line width−peak energy slope.

On the other side, our simple model allows correct reproduction of (1) the linear line width increase at low emission energy; (2) the saturation at high emission energy; (3) the energy range of the plateau at high energy; and (4) the energy range of the maximum spectral narrowing, consistent also with the results of ref 40.

Nevertheless, we would like to underline once more that the results of the proposed model, which is clearly approximate, have to be intended just as a qualitative confirmation of our explanation of the experimental results on the local variation of the fluorescence spectra. In order to have a quantitative model, uphill migration has to be included as the fluorescence line width is on the order of the thermal energy. This can be done by numerical techniques,[8] but it is beyond the scope of the present paper.

IV. Conclusions

In conclusion, we employed confocal laser spectroscopy to investigate the microscopic fluorescence properties of a non-uniform PF8 thin film containing both the glassy and β phase.

We showed that considerable differences in the fluorescence spectra are present in different samples regions on the micron size scale. In particular, in relation to microscopic morphology irregularities, the fluorescence spectra of the PF8 β-phase result considerably red-shifted and narrowed with respect to the one collected in the uniform morphology region of the sample. We concluded that the higher surface energy in relation to microscopic morphological irregularities affects the PF8−toluene vapor interaction, resulting in a higher β-phase volumetric density. Thus, in these regions, intermolecular energy migration within the β-phase excited-state distribution is progressively switched on, leading to a PL red shift up to 26 meV and narrowing up to 18 meV.

Acknowledgment. The authors would like to acknowledge Roberto Cingolani and Giuseppe Gigli of NNL for the use of their experimental facilities, Andrea Ventura of the GAMPA group, and Adriana Passaseo of NNL for useful discussions.

References and Notes

(1) Tessler, N.; Denton, G. J.; Friend, R. H. *Nature* **1996**, *382*, 695.
(2) Burroughes, J. H.; Bradley, D. D. C.; Brown, A. R.; Marks, R. N.; Mackay, K.; Friend, R. H.; Burns, P. L.; Holmes, A. B. *Nature* **1990**, *347*, 539.
(3) Assadi, A.; Svensson, C.; Willander, M.; Ingänas, O. *Appl. Phys. Lett.* **1988**, *53*, 195.
(4) Sariciftci, N. S.; Braun, D.; Zhang, C.; Srdanov, V. I.; Heeger, A. J.; Stucky, G.; Wudl, F. *Appl. Phys. Lett.* **1993**, *62*, 585.
(5) Hepp, A.; Heil, H.; Weise, W.; Ahles, M.; Schmechel, R.; von Seggern, H. *Phys. Rev. Lett.* **2003**, *91*, 157406.
(6) Kersting, R.; Lemmer, U.; Mahrt, R. F.; Leo, K.; Kurz, H.; Bässler, H.; Göbel, E. O. *Phys. Rev. Lett.* **1993**, *70*, 3820.
(7) Mollay, B.; Lemmer, U.; Kersting, R.; Mahrt, R. F.; Kurz, H.; Kauffmann, H. F.; Bässler, H. *Phys. Rev. B* **1994**, *50*, 10769.
(8) Meskers, S. C. J.; Hübner, J.; Oestreich, M.; Bässler, H. *J. Phys. Chem. B* **2001**, *105*, 9139.
(9) Tsutsumi, N.; Fujihara, A.; Hayashi, D. *Appl. Opt.* **2006**, *45*, 5748.
(10) Tasch, S.; List, E. J. W.; Ekström, O.; Graupner, W.; Leising, G.; Schlichting, P.; Rohr, U.; Geerts, Y.; Scherf, U.; Müllen, K. *Appl. Phys. Lett.* **1997**, *71*, 2883.
(11) List, E. J. W.; Creely, C.; Leising, G.; Schulte, N.; Schluter, A. D.; Scherf, U.; Mullen, K.; Graupner, W. *Chem. Phys. Lett.* **2000**, *325*, 132.
(12) Herz, L. M.; Silva, C.; Grimsdale, A. C.; Müllen, K.; Phillips, R. T. *Phys. Rev. B* **2004**, *70*, 165207.
(13) Haugeneder, A.; Neges, M.; Kallinger, C.; Spirkl, W.; Lemmer, U.; Feldmann, J.; Scherf, U.; Harth, E.; Gügel, A.; Müllen, K. *Phys. Rev. B* **1999**, *59*, 15346.
(14) Heller, C. M.; Campbell, I. H.; Laurich, B. K.; Smith, D. L.; Bradley, D. D. C.; Burn, P. L.; Ferraris, J. P.; Müllen, K. *Phys. Rev. B* **1996**, *54*, 5516.
(15) List, E. J. W.; Guentner, R.; Scanducci Freitas, P.; Scherf, U. *Adv. Mater.* **2002**, *14*, 374.
(16) Grazulevicius, J. V.; Soutar, I.; Swanson, L. *Macromolecules* **1998**, 31, 4820.
(17) Yokoyama, M.; Akiyama, K.; Yamamori, N.; Mikawa, H.; Kusabayashi, S. *Polym. J.* **1985**, *17*, 545.
(18) Kwak, E.-S.; Vanden Bout, D. A. *Anal. Chim. Acta* **2003**, *496*, 259.
(19) Cadby, A.; Dean, R.; Fox, A. M.; Jones, R. A. L.; Lidzey, D. G. *Nano Lett.* **2005**, *5*, 2232.
(20) Cadby, A.; Dean, R.; Fox, A. M.; Jones, R. A. L.; Lidzey, D. G. *Adv. Mater.* **2006**, *18*, 2713.
(21) Cadby, A. J.; Dean, R.; Elliot, C.; Jones, R. A. L.; Fox, A. M.; Lidzey, D. G. *Adv. Mater.* **2007**, *19*, 107.
(22) Teetsov, J.; Vanden Bout, D. A. *J. Phys. Chem. B* **2000**, *104*, 9378.
(23) Teetsov, J.; Vanden Bout, D. A. *J. Am. Chem. Soc.* **2001**, *123*, 3605.
(24) Kwak, E.-S.; Kang, T. J.; Vanden Bout, D. A. *Anal. Chem.* **2001**, *73*, 3257.
(25) Loi, M. A.; da Como, E.; Dinelli, F.; Murgia, M.; Zamboni, R.; Biscarini, F.; Muccini, M. *Nat. Mater.* **2005**, *4*, 81.
(26) Caruso, M. E.; Lattante, S.; Cingolani, R.; Anni, M. *Appl. Phys. Lett.* **2006**, *88*, 181906.
(27) Bernius, M. T.; Inbasekaran, M.; O'Brien, J.; Wu, W. S. *Adv. Mater.* **2000**, *12*, 1737.
(28) Grice, A. W.; Bradley, D. D. C.; Bernius, M. T.; Inbasekaran, M.; Wu, W. W.; Woo, E. P. *Appl. Phys. Lett.* **1998**, *73*, 629.
(29) Halls, J. J. M.; Arias, A. C.; Mackenzie, J. D.; Wu, W. S.; Inbasekaran, M.; Woo, E. P.; Friend, R. H. *Adv. Mater.* **2000**, *12*, 498.
(30) Sirringhaus, H.; Wilson, R. J.; Friend, R. H.; Inbasekaran, M.; Wu, W.; Woo, E. P.; Grell, M.; Bradley, D. D. C. *Appl. Phys. Lett.* **2000**, *77*, 406.
(31) Heliotis, G.; Xia, R.; Bradley, D. D. C.; Turnbull, G. A.; Samuel, I. D. W.; Andrew, P.; Barnes, W. L. *Appl. Phys. Lett.* **2003**, *83*, 2188.
(32) Heliotis, G.; Xia, R.; Bradley, D. D. C.; Turnbull, G. A.; Samuel, I. D. W.; Andrew, P.; Barnes, W. L. *J. Appl. Phys.* **2004**, *96*, 6959.
(33) Heliotis, G.; Xia, R.; Turnbull, G. A.; Piers, A.; Barnes, W. L.; Samuel, I. D. W.; Bradley, D. D. C. *Adv. Func. Mater.* **2004**, *14*, 91.
(34) Zaumseil, J.; Donley, C. L.; Kim, J.-S.; Friend, R. H.; Sirringhaus, H. *Adv. Mater.* **2006**, *18*, 2708.
(35) Winokur, M. J.; Slinker, J.; Huber, D. L. *Phys. Rev. B* **2003**, *67*, 184106.
(36) Scherf, U.; List, E. J. W. *Adv. Mater.* **2002**, *14*, 477.
(37) Grell, M.; Bradley, D. D. C. *Adv. Mater.* **1999**, *11*, 895.
(38) Khan, A. L. T.; Sreerunothai, P.; Herz, L. M.; Banach, M. J.; Köhler, A. *Phys. Rev. B* **2004**, *69*, 085201.
(39) Cadby, A. J.; Lane, P. A.; Mellor, H.; Martin, S. J.; Grell, M.; Giebeler, C.; Bradley, D. D. C.; Wohlgenannt, M.; An, C.; Vardeny, Z. V. *Phys. Rev. B* **2000**, *62*, 15604.
(40) Ariu, M.; Sims, M.; Rahn, M. D.; Hill, J.; Fox, A. M.; Lidzey, D. G.; Oda, M.; Cabanillas-Gonzales, J.; Bradley, D. D. C. *Phys. Rev. B* **2003**, *67*, 195333.
(41) Chunwaschirasiri, W.; Tanto, B.; Huber, D. L.; Winokur, M. J. *Phys. Rev. Lett.* **2005**, *94*, 107402.
(42) Hayer, A.; Khan, A. L. T.; Friend, R. H.; Köhler, A. *Phys. Rev. B* **2005**, *71*, 241302.
(43) Korovyanko, O. J.; Vardeny, Z. V. *Chem. Phys. Lett.* **2002**, *356*, 361.
(44) Rothe, C.; Galbrecht, F.; Sherf, U.; Monkman, A. *Adv. Mater.* **2006**, *18*, 2137.
(45) Briseno, A. L.; Mannsfeld, S. C. B.; Ling, M. M.; Liu, S.; Tseng, R. J.; Reese, C.; Roberts, M. E.; Yang, Y.; Wudl, F.; Bao, Z. *Nature* **2006**, *444*, 913.
(46) Venables, J. A.; Spiller, G. D. T.; Hanbucken, M. *Rep. Prog. Phys.* **1984**, *47*, 399.
(47) Gránásy, L.; Börzsönyi, T.; Pusztai, T. *Phys. Rev. Lett.* **2002**, *88*, 206105.
(48) Caruso, M. E.; Anni, M. *Phys. Rev. B* **2007**, *76*, 054207.
(49) Harkema, S.; Schaffer, E.; Morariu, M. D.; Steiner, U. *Langmuir* **2003**, *19*, 9714.
(50) Chi, C.; Wegner, G. *Macromol. Rapid Commun.* **2005**, *26*, 1532.
(51) The density of the PF8 film has been estimated to be about 2×10^{20} molecule cm^{-3} assuming a mass density of 1 g cm^{-3} and the average conjugation length reported in ref 50.
(52) Müller, J. G.; Lemmer, U.; Raschke, G.; Anni, M.; Scherf, U.; Feldmann, J.; Lupton, J. M. *Phys. Rev. Lett.* **2003**, *91*, 267403.
(53) Bässler, H.; Schweitzer, B. *Acc. Chem. Res.* **1999**, *32*, 173.